University of Kent

Kent Academic Repository

Abdulsada, Hazim A, Assimakopoulos, Philippos, Vieira, Luis C. and Gomes, Nathan J. (2026) *Performance of DPD training approaches for optical mobile fronthaul with analog transport*. Optics Communications, 623 . ISSN 0030-4018.

Downloaded from
https://kar.kent.ac.uk/116771/ The University of Kent's Academic Repository KAR

The version of record is available from
https://doi.org/10.1016/j.optcom.2026.133824

This document version
Author's Accepted Manuscript

DOI for this version

Licence for this version
CC BY (Attribution)

Additional information
For the purpose of open access, the author(s) has applied a Creative Commons Attribution (CC BY) licence to any Author Accepted Manuscript version arising

Versions of research works

Versions of Record
If this version is the version of record, it is the same as the published version available on the publisher's web site. Cite as the published version.

Author Accepted Manuscripts
If this document is identified as the Author Accepted Manuscript it is the version after peer review but before type setting, copy editing or publisher branding. Cite as Surname, Initial. (Year) 'Title of article'. To be published in ***Title of Journal*** , Volume and issue numbers [peer-reviewed accepted version]. Available at: DOI or URL (Accessed: date).

Enquiries
If you have questions about this document contact ResearchSupport@kent.ac.uk. Please include the URL of the record in KAR. If you believe that your, or a third party's rights have been compromised through this document please see our Take Down policy (available from https://www.kent.ac.uk/guides/kar-the-kent-academic-repository#policies).

Performance of DPD Training Approaches for Optical Mobile Fronthaul with Analog Transport

Hazim A. Abdulsada[a,*], Philippos Assimakopoulos[a], Luis C. Vieira[b], and Nathan J. Gomes[a,c], *Senior Member, IEEE*

[a*]*Hazim Abdulwahhab Abdulsada and Philippos Assimakopoulos, School of Engineering, Mathematics and Physics, University of Kent, CT2 7NZ Canterbury, U.K, (e-mail: ha495@kent.ac.uk; p.asimakopoulos@kent.ac.uk).*
[b]*Luis C, Vieira, Department of Electronics (DAELN-CT), Federal University of Technology-Parana (UTFPR), Curitiba 80230-901, Brazil, e-mail: vieira@utfpr.edu.br.*
[a,c]*Nathan J. Gomes, Department of Electronic and Electrical Engineering, University College London, WC1E 6BT London, U.K., e-mail: n.j.gomes@ucl.ac.uk.*
*Corresponding author.

Abstract

A scalable and complexity-aware Digital Predistortion (DPD) training framework is proposed and analyzed for optical mobile fronthaul transporting wide-bandwidth channels. The framework incorporates conventional per-channel training approaches together with a Nyquist Zone (NZ)-based approach for DPD training and coefficient estimation which reduces feedback and implementation complexity by building on the NZ mapping concept for grouping channels. Results show that training approaches employing both per-channel memory and nonlinear coefficient estimation achieve the best Error Vector Magnitude (EVM) performance. The proposed NZ-based approach, however, achieves comparable EVM performance for an eight-channel multiplex using four NZs, thereby reducing coefficient estimation complexity by 50% together with its associated power consumption. Thus, the proposed DPD training approach provides an attractive trade-off between linearization performance and implementation complexity for analog mobile fronthaul.

Keywords: Radio-over-Fiber (RoF), Subcarrier Multiplexing (SCM), Mobile Fronthaul, Optical Fronthaul, Digital Signal Processing (DSP), Digital Predistortion (DPD)

1. Introduction

Next-generation Radio Access Networks (RANs) require fronthaul links supporting significantly higher bit-rates while meeting increasingly stringent latency constraints [1-6]. Traditional Digital Radio-over-Fiber (DRoF) solutions based on the transport of digitized I/Q samples, such as the Common Public Radio Interface (CPRI), become increasingly impractical for beyond-5G systems, where fronthaul rates can reach hundreds of Gb/s or even Tb/s due to increasing signal bandwidths and antenna counts [6].

To address these challenges, functional-split RAN architectures distribute portions of the baseband processing between the Distributed Unit (DU) and Remote Unit (RU), reducing fronthaul bit-rates at the expense of increased latency and reduced centralization benefits [6-8]. Alternatively, analog fronthaul preserves centralization by transporting radio signals directly in the analog domain [6], [9], [10]. DSP-assisted Subcarrier Multiplexing (SCM) further enables flexible aggregation and transport of multi-band radio signals, providing scalability across numerologies, and modulation formats [11], [12]. However, analog transport remains susceptible to nonlinear impairments including those arising from components in an optical link, which can significantly degrade signal quality and system performance, particularly under high-power operating conditions [13-19]. Although linearization techniques such as Digital Predistortion (DPD) can mitigate these effects, implementation complexity remains a major challenge [17].

Considerable effort has therefore been devoted to reducing DPD implementation complexity through bandwidth reduction, undersampling techniques, and simplified coefficient estimation methods [18]. Nevertheless, in multichannel DPD systems the number of coefficients typically scales with the number of channels, making conventional approaches increasingly impractical for wideband multi-channel operation [18], [20], [21]. As signal bandwidths and sampling rates increase, processor workload and power consumption become dominated by the DSP sampling rate, motivating the need for complexity- and power-aware DPD implementations [22], [23].

Several nonlinear dynamic DPD models have been proposed for analog transport systems, including Volterra, Generalized Memory Polynomial (GMP), Canonical Piecewise Linearization (CPWL), neural-network-based, and Memory Polynomial (MP) approaches [13], [15], [23-26]. While Volterra, CPWL and neural-network techniques can provide excellent linearization performance, they incur substantial implementation complexity [13], [23-24]. GMP offers a lower-complexity alternative, but MP remains particularly attractive due to its reduced

coefficient count, efficient least-squares estimation, and favorable complexity-performance trade-off [25-27]. In fronthaul applications, where low cost, power efficiency and scalability are essential, such complexity considerations are especially important [22].

Beyond the DPD model itself, the adaptive training algorithm also affects implementation complexity. Least-Mean-Square (LMS) and Recursive Least-Squares (RLS) are the most widely used approaches; however, although RLS converges faster, its computational cost and numerical sensitivity often limit practical deployment. Consequently, LMS-based techniques are typically preferred, providing a balanced trade-off between performance and implementation feasibility [28].

This paper proposes and investigates a scalable and complexity-aware training approach for low-complexity MP-based DPD in DSP-assisted analog mobile fronthaul systems. The key contribution is an Nyquist Zone (NZ)-based DPD training approach that builds on the existing concept of NZ mapping as the basis for grouping channels. In this approach, DPD training, feedback acquisition, and coefficient updating are performed on a per-zone rather than a per-channel basis. By exploiting the inherent structure of NZ-based signal organization, the proposed approach reduces feedback requirements and coefficient-update complexity with the goal of retaining the performance of channel-specific memory compensation.

Unlike prior work that primarily focuses on developing new DPD models, the objective of this work is to optimize how DPD training is performed in practical high-bandwidth multi-channel fronthaul systems. Several DPD training approaches are compared in terms of Error Vector Magnitude (EVM) performance, computational complexity and power consumption for a DSP-enabled optical mobile fronthaul transporting up to eight 3GPP-compliant channels [29], with bandwidths of 100 MHz and 400 MHz. The rest of the paper is organized as follows. Section 2 presents the system model for the DPD training technique within a DSP-assisted fronthaul, including implementation and modeling. Section 3 details the simulation and measurement setup and evaluates three DPD training approaches. Section 4 introduces the NZ-based DPD training approach and its verification through simulations. Section 5 provides DPD complexity and power prediction, while Section 6 concludes the paper.

2. Predistortion Training Approaches in the DSP-Assisted Optical Mobile Fronthaul

This section describes the system architecture and the DPD training approaches considered in this work. Subsection 2.1 introduces the conceptual downlink architecture for DSP-assisted Optical Mobile fronthaul and outlines the associated signal generation and processing flow between the DU and the RU. Subsection 2.2 then presents the different DPD training approaches investigated, providing a comparative overview of their operating principles.

2.1. DSP-Assisted Optical Mobile Fronthaul

A conceptual view of the downlink section of the DSP-assisted optical fronthaul, derived from [11], is illustrated in Fig. 1. Baseband Quadrature Amplitude Modulation (QAM) symbols are first generated by the digital modulation block, after which numerology-specific multiplexing is applied. The resulting data stream is transformed into the time domain through an Inverse Fast Fourier Transform (IFFT), followed by Parallel-to-Serial conversion (P/S) and Cyclic-Prefix (CP) insertion.

Multiple channels (or groups of channels) are generated by parallel IFFT processes, and the final multiplex is created by passing each channel (or channel group) through a Digital Up-Converter (DUC) and summing outputs to create the composite SCM signal. The versatility in allowing a single IFFT process for the multiplexing of multiple channels (i.e., a channel group) in the frequency domain (e.g., channels that comprise the same numerology) enables the production of sub-multiplexes of varying sizes, with each single-IFFT output created such that frequency domain guard bands exist in spaces between the channels [11], [16]. The final multiplex is converted to the analog domain for optical link transmission by a Digital-to-Analog Converter (DAC). Depending on the DPD training approach to be applied, DPD modules may be placed before or after the summation of the channels that creates the composite multiplex, as shown in Fig. 1.

Following analog transport over the fronthaul, the RU captures the transmitted analog waveform and digitizes it using an Analog-to-Digital Converter (ADC). The digitized signal is then processed by one or more Digital Down-Conversion (DDC) modules, which shift the waveform to baseband, apply decimation, and isolate the relevant carriers or numerology components required for DPD training. Each branch then undergoes CP removal, Serial-to-Parallel (S/P) conversion and Fast Fourier Transform (FFT) processing, followed by numerology-specific de-multiplexing and digital demodulation to recover the transmitted data streams.

The Extract Training Signals block in the RU provides the feedback for the DPD Training & Coefficient Extraction block in the DU to estimate the nonlinear characteristics and memory effects of the optical link. In a real system this feedback would be provided through the uplink transmission.

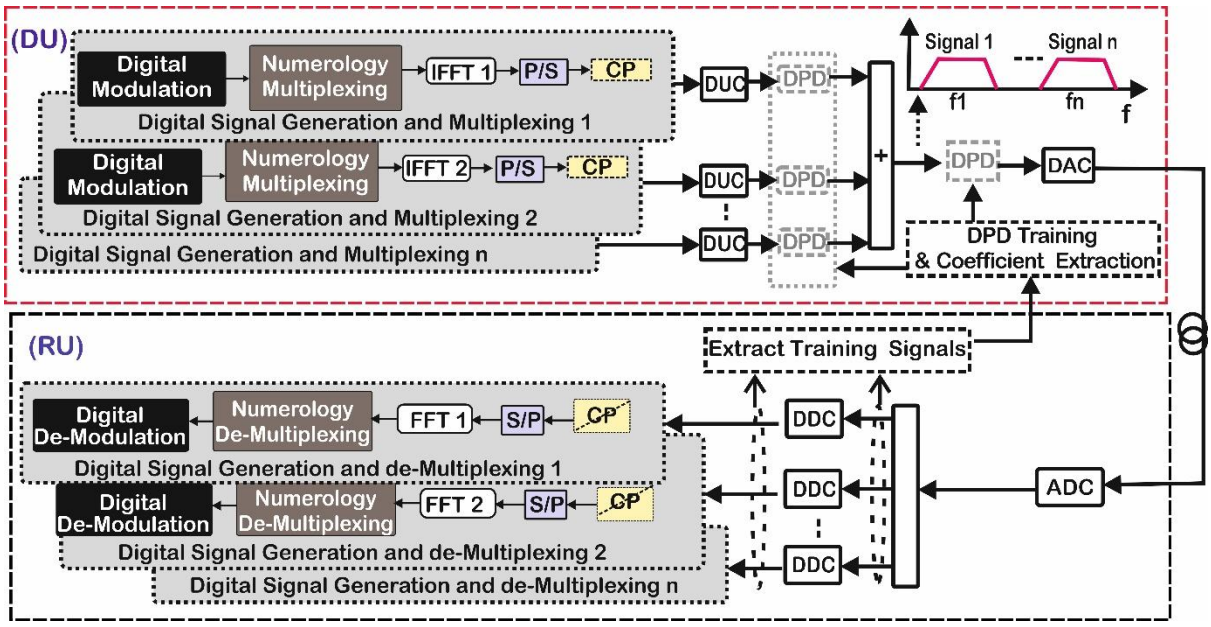


Fig. 1. Conceptual view of Distributed Unit (DU) and Remote Unit (RU) processes for the downlink DSP-assisted optical mobile fronthaul with DPD. DUC, Digital-Up-Converter; DDC, Digital Downconverter; DAC, Digital-to-Analogue Converter; CP, Cyclic Prefix; ADC, Analogue-to-Digital Converter; PS, parallel to serial; S/P, serial to parallel; IFFT, Inverse Fast Fourier Transform; FFT, Fast Fourier Transform.

The training process itself, which is the most computationally demanding step, is performed outside the fronthaul data path as it is not applied continuously. Real-time updates to the DPD correction parameters are not necessary, as the nonlinearity in an analog optical link is expected to change slowly over time [30], [31]. Consequently, the proposed architecture is expected to meet the latency and reliability requirements anticipated for future 6G networks.

2.2. DPD Training Approach Types

Throughout this work, the DPD is performed using a MP least-squares-based identification technique as described in [27]. The investigated Composite Multiplex-based DPD (CM-DPD) training approach is represented at top-left of Fig. 2 (A). With this approach the whole composite signal/multiplex is transmitted during training, and the extracted predistortion coefficients (which include both memory coefficients (Q) and nonlinear coefficients (K)) are applied to the whole composite signal/multiplex (at top-right of Fig. 2 (B)).

Fig. 2 (A) at bottom-left, depicts the Single Channel-based DPD (SC-DPD) training approach. With this approach, training is conducted on one-channel and the extracted coefficients are subsequently applied to the whole composite signal/multiplex (at bottom-right in Fig. 2 (B)). For example, only the first channel of the multiplex is transmitted for training, and the corresponding extracted coefficients (again, including both memory and nonlinear coefficients) are then used to predistort all N channels in the multiplex before transmission. Both CM-DPD and SC-DPD training approaches employ a single predistorter for the composite signal/multiplex.

Fig. 3 (A) illustrates a hybrid DPD training approach. The hybrid DPD remains a waveform-based predistortion technique using time-domain waveform samples for training, while differing from CM-DPD in its coefficient-identification strategy. The approach is termed hybrid because: (1) Each channel is trained independently to extract channel-specific memory coefficients (Q1-QN), which are then applied (Fig. 3 (B), right side) on a per-channel basis; (2) A single predistorter uses a common set of nonlinear coefficients (K1) estimated from one channel during training and applies them to the whole composite signal/multiplex. As a result, this approach results in an amount of feedback proportional to (N+1), where N is the number of channels in the multiplex.

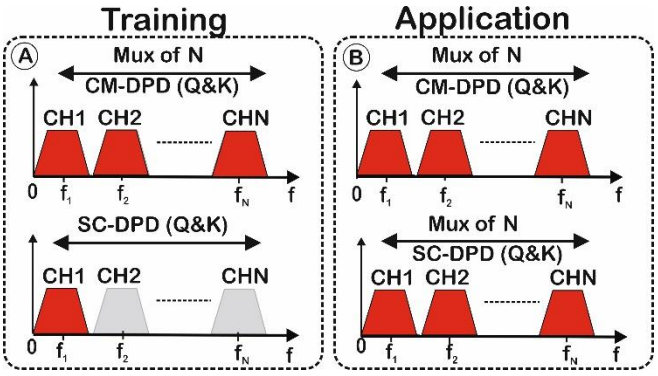


Fig. 2 Conceptual depiction of the CM-DPD and SC-DPD training and application workflows. Left (A): channels used for training (CM-DPD, top; SC-DPD, bottom). Right (B): application of the extracted coefficients to CM-DPD (top) and SC-DPD (bottom). (Q) denotes memory coefficients and (K) nonlinear coefficients. Dark red is an active channel; light grey is an inactive channel.

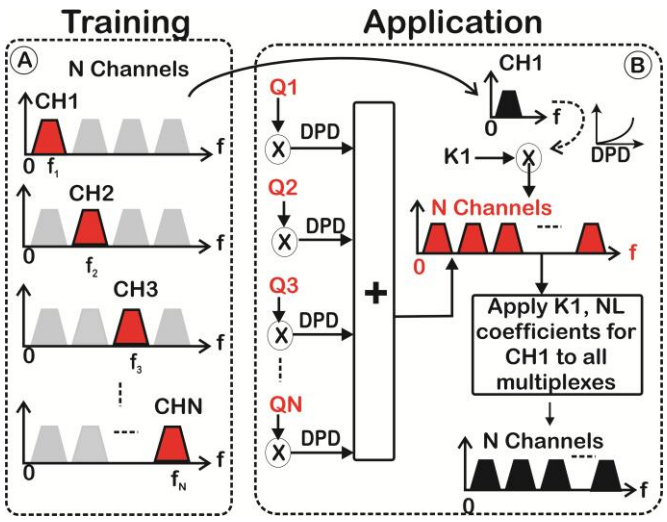


Fig. 3. Conceptual depiction of the hybrid DPD training approach. Q1-QN represents the extracted memory coefficients. Specifically, Q1, Q2, Q3, and QN correspond to the memory coefficients for channels CH1, CH2, CH3, and CHN, respectively, while K1 denotes amplitude nonlinearity coefficients extracted from CH1. The left (A) represents the channels being used for the training, whereas the right (B) represents how the extracted coefficients are applied. Dark red is an active channel; light grey is an inactive channel.

3. Simulation, Measurement Set-up and Performance Evaluations

This section presents the performance evaluation of the proposed DPD training approaches using both numerical simulations and experimental measurements. Subsection 3.1 describes the simulation setup and corresponding performance assessment for the different DPD training approaches. Subsection 3.2 details the experimental setup and validation, demonstrating practical effectiveness under real hardware conditions.

3.1. Simulation Setup and Performance Evaluation

Fig. 4 depicts the MATLAB-VPI (Virtual Photonics Inc.) co-simulation environment that is employed. VPI orchestrates the overall simulation and invokes MATLAB-based transmitter processing functions, which generate frequency-domain QAM samples, insert pilots for tracking the channel frequency response, and perform multiplexing. The resulting waveform samples are then passed to the VPI optical fiber link model. For the receiver side processing, the sample streams obtained from the VPI-modelled optical link are transferred back to MATLAB, where several signal processing steps are performed, including demultiplexing, downconversion of each channel to baseband through DDCs, per-channel FFT, frequency-domain equalization and demodulation, followed by EVM estimation.

At the top of Fig. 4, the feedback path for the predistorter training interface is shown, which provides access to the DPD training & coefficient extraction block associated with the various DPD training approaches.

Following training, the extracted coefficients are used to predistort a newly generated composite signal/multiplex.

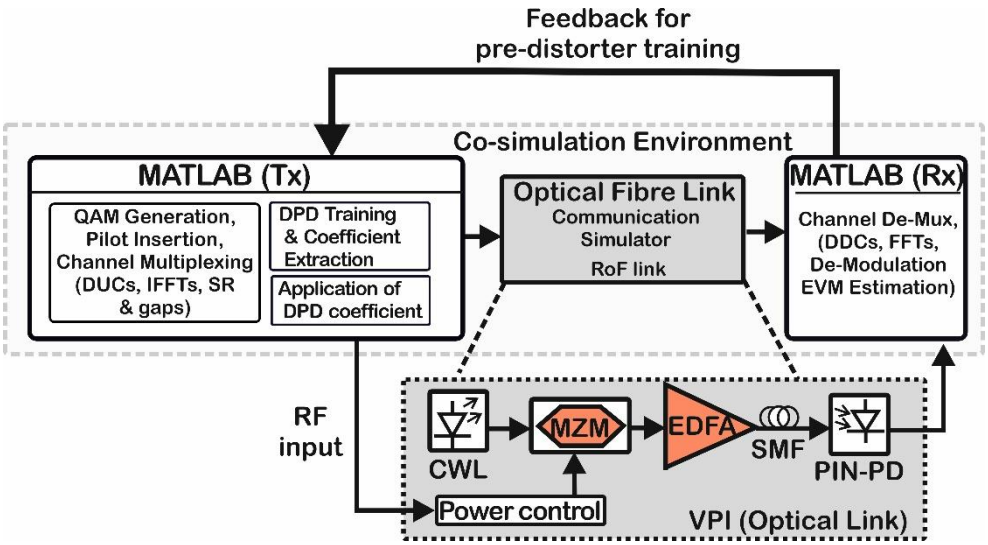


Fig. 4. Co-simulation environment for generation and reception of composite signals/multiplexes, DPD coefficient estimation and predistortion. MZM, Mach-Zehnder Modulator; EDFA, Erbium-Doped Fiber Amplifier; SMF, Single-Mode Fiber; CWL, Continuous-Wave Laser, PD, Photo Diode.

The optical fiber link used in the simulation, depicted in the lower part of Fig. 4, consists of a Mach-Zehnder Modulator (MZM) fed by a Continuous-Wave Laser (CWL). The modelled optical link has a 1-dB compression point of 16 dBm and has been previously benchmarked to a laboratory setup [32]. The optical signal at the MZM output is amplified by an Erbium-Doped Fiber Amplifier (EDFA), transmitted through a short-length Single-Mode Fiber (SMF) patch cord (in this case), and subsequently detected by a PIN photodiode (PIN-PD). Under the operating conditions considered, the dominant nonlinear impairment originates from the optical modulator, while chromatic-dispersion- and fiber-nonlinearity-induced distortions remain comparatively small for short-reach optical fronthaul fiber links (of up to 10 km) [33], [34].

Two signal bandwidth configurations are investigated: the first employs a channel bandwidth of 100 MHz with a per-channel sampling rate of 122.88 MSps, while the second utilizes a channel bandwidth of 400 MHz with a per-channel sampling rate of 491.52 MSps. In the 100 MHz configuration, the signal comprises 3120 data subcarriers and 976 null subcarriers for a per-channel IFFT size of 4096 and subcarrier spacing (SCS) of 30 kHz. For the 400 MHz configuration, the signal contains 792 data subcarriers and 232 null subcarriers for a per-channel IFFT of 1024 and SCS of 480 kHz. Note that the choice of an IFFT size of 1024 for the 400 MHz BW case was made in agreement with the 3GPP specification [35]. Simulations carried out with the larger IFFT size of 4096 (120 kHz SCS) for the 400 MHz bandwidth case (not shown here) show that this choice has a negligible impact on EVM performance. Both configurations use 16-QAM modulation. Across all multiplexed channels considered in this study, a fixed inter-channel guard band of 10 MHz is maintained. For DPD modelling, Q=5 and K=5 are selected as a compromise between modelling capability and implementation complexity.

Fig. 5 shows per-channel EVM results for the three DPD training approaches, for a channel multiplex comprising four 100 MHz channels, with the first channel in the multiplex centered at a carrier frequency of (a) 50 MHz and (b) 1200 MHz, and four 400 MHz channels, with the first channel centered at a carrier frequency of (c) 200 MHz and (d) 1200 MHz. The per-channel EVM is given as the percentage (%) Root-Mean Square (RMS) value, averaged across all subcarriers of each channel within the multiplex. All DPD approaches improve EVM relative to the No-DPD case. CM-DPD and SC-DPD exhibit similar performance, with slightly improved linearization at higher carrier frequencies due to reduced influence of near-DC second-order Intermodulation (IMD2) products. By employing independent memory representations for each channel (unlike CM-DPD and SC-DPD) the hybrid approach maintains per-channel EVM below 5% and 7%, for the 100 MHz and 400 MHz bandwidth cases, respectively.

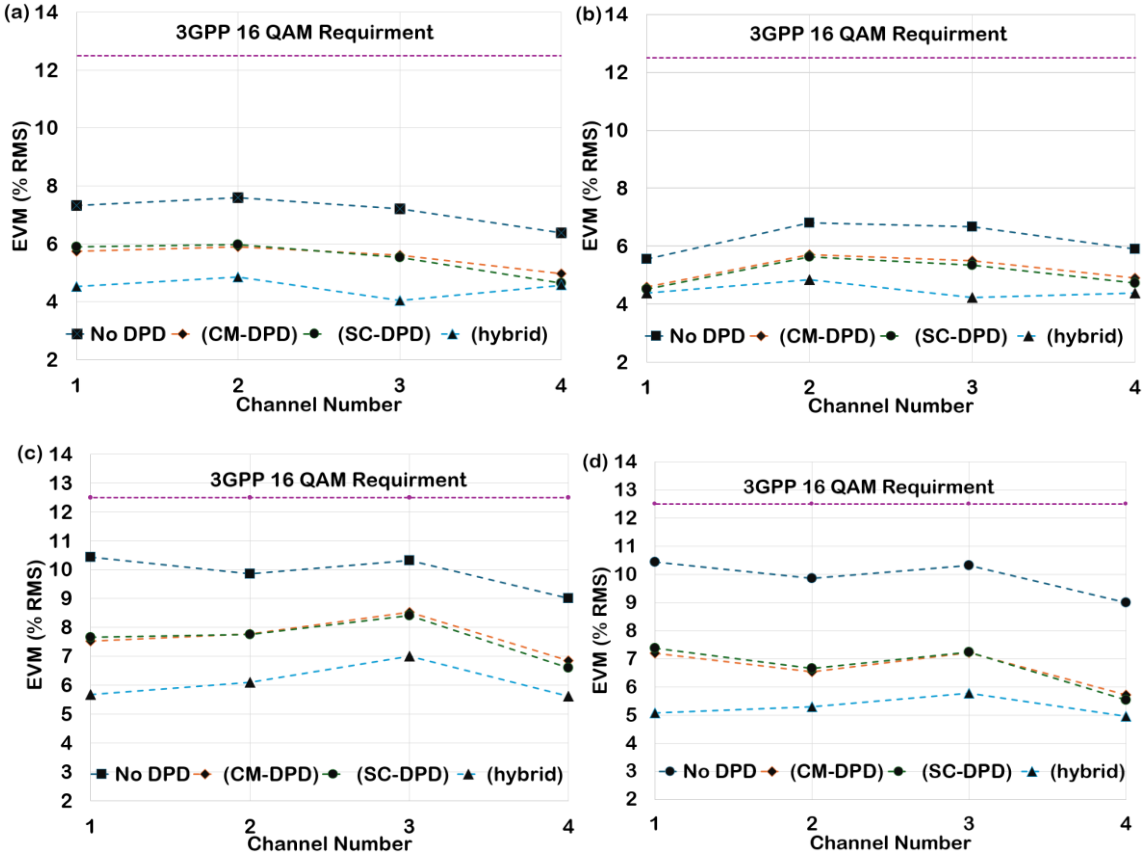


Fig. 5. Per-channel Error Vector Magnitude (EVM, % RMS) for 16 QAM modulation, before and after DPD for a signal multiplex comprising four channels, with a total input power (Pin) of 19 dBm. (a) 100 MHz channel bandwidths, with the first channel centered at 50 MHz. (b) 100 MHz channel bandwidths, with the first channel centered at 1200 MHz. (c) 400 MHz channel bandwidths, with the first channel centered at 200 MHz.(d) 400 MHz channel bandwidths, with the first channel centered at 1200 MHz. Dashed lines are used only to associate results for similar systems and do not indicate trends between adjacent points.

Note that the observed trends are expected to remain valid for practical fronthaul fiber lengths (of up to 10 km) [33], [34]. The hybrid approach separates nonlinear coefficient estimation from memory coefficient estimation. The single-channel nonlinear estimation employed in the hybrid approach generalizes effectively to multi-channel multiplexes, as single-channel and aggregated multi-channel signals exhibit similar amplitude distributions and Peak-to-Average Power Ratio (PAPR) characteristics [36]. Consequently, the nonlinear coefficients obtained from a single-channel training signal are expected to remain representative of the composite multiplex since practical fronthaul fiber lengths have negligible impact on these signal statistics. In contrast, memory coefficients are estimated independently for each channel. Therefore, memory effects arising from the frequency-dependent phase response introduced by fiber propagation are incorporated within the per-channel memory estimation stage.

3.2. Experiment Setup and Measurement Results

Fig. 6 depicts the experimental setup employed for per-channel EVM measurements for two of the DPD training approaches (CM-DPD and hybrid). (As the simulation results in Fig. 5 showed that SC-DPD training exhibited per-channel EVM performance comparable to CM-DPD, further experimental investigation was not considered necessary). Due to current limitations in the available laboratory equipment, the optical link for these experiments is different to that used for the co-simulation-based investigation presented in Subsection 3.1, but has also been benchmarked for simulations in [37]. The experimental Directly Modulated Laser (DML)-Distributed Feedback (DFB) link introduces laser chirp not explicitly captured by the MZM-based simulation, however, its impact is expected to be limited for the <10-km links considered here, given the comparable DPD performance reported for DML-DFB- and MZM-based RoF links [38], and the limited chirp-dispersion effects at short reaches [15], [39]. Moreover, any chirp-related distortion in the experimental DML-DFB link is inherently captured by the measured input-output response used for MP-DPD identification. Other than the optical link, the remaining procedures (generation, reception and decoding of signals) employ the same MATLAB processing blocks as with

the co-simulation system presented in Subsection 3.1, with the inclusion of time correction at the MATLAB (Rx) side.

The generated signal is converted to the time domain to produce I/Q samples, which are downloaded to a Tektronix AWG7122C Arbitrary Waveform Generator (AWG). The AWG performs digital-to-analog conversion and its analog output is connected to an electronic amplifier (A1). This amplified signal is then passed to a power control unit, which precisely regulates the drive power to the Radio-Frequency (RF) input of a DML-Teradian DFB laser. The resulting modulated optical signal is then transmitted over a short-length (approx. 1 m) fiber patchcord. The detected signal at the PD is first amplified by the second electronic amplifier (A2) and then captured using a Tektronix 72304DX Digital Phosphor Oscilloscope (DPO). The optical link has a 1 dB compression point of 18 dBm. Finally, the captured signal is processed offline by the MATLAB (Rx). The demultiplexing process is common across both DPD training approaches and is implemented using DDCs.

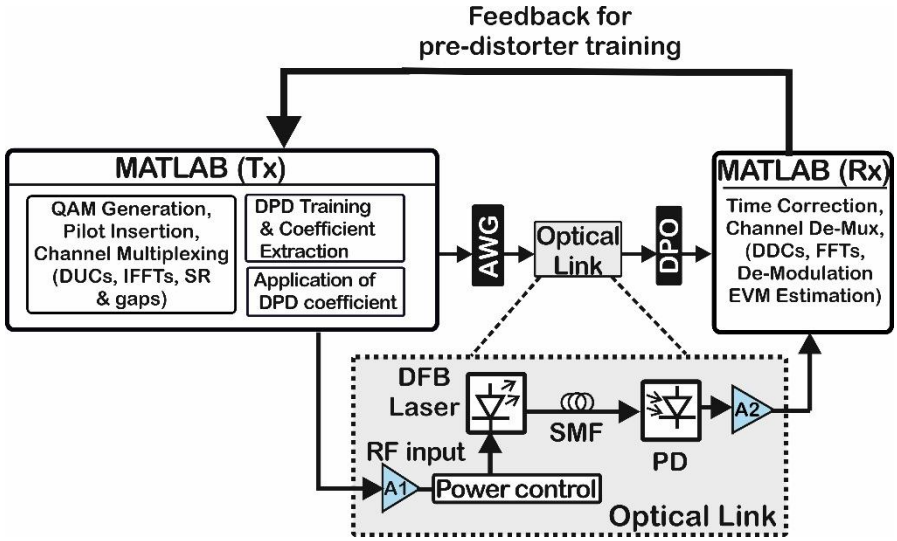


Fig. 6. Experimental setup for EVM measurements. AWG, Arbitrary Waveform Generator; DPO, Digital Phosphor Oscilloscope; DFB, Distributed Feedback Laser; A1, Electronic Amplifier 1; SMF, Single-Mode Fiber; PD, Photodiode; A2, Electronic Amplifier 2.

Two experiments have been carried out. In the first experiment, a bandwidth of approximately 100 MHz was employed, based on a subcarrier spacing of 30 kHz, with 3120 data subcarriers and 976 null subcarriers. This configuration matches the 100 MHz simulation presented in Subsection 3.1. In the second experiment, a bandwidth of 74.38 MHz was employed, serving as an additional verification of the employed approach, based on a generic subcarrier spacing of 23.84 kHz, with 3120 data subcarriers and 976 null subcarriers. The reduced bandwidth was selected due to sampling-rate compatibility between the AWG and DPO and the bandwidth limitations of the available RF amplifiers, ensuring reliable signal acquisition and decoding. Both experiments involve the transmission of four equally-spaced channels with a total sampling rate of 3.125 GSps and a first carrier frequency centered at 50 MHz while the input power to the DFB laser is 18 dBm. The results presented in Fig. 7(a) show that, for a signal bandwidth of 74.38 MHz, the hybrid DPD training approach (average EVM of 5.3%, compared to 11.8% without DPD) achieves lower EVM compared to the CM-DPD training approach. For the higher channel bandwidth of 100 MHz, the hybrid DPD training approach again demonstrates lower EVM (average EVM of 6.8%, compared to 11.4% without DPD) compared to the CM-DPD training approach, as shown in Fig. 7(b). These results therefore, are in general agreement with the simulation results presented in Fig. 5.

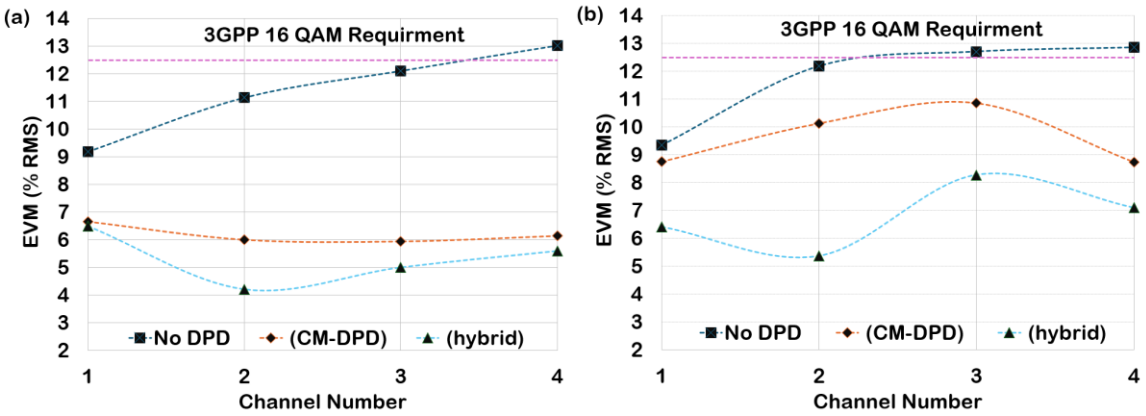


Fig. 7. Per-channel Error Vector Magnitude (EVM, % RMS) measurement results for 16 QAM modulation, before and after DPD for a signal multiplex. comprising four channels, at an input power of 10 dBm. (a) 74.38 MHz channel bandwidth, and (b) 100 MHz channel bandwidth. In both cases, the first channel is centered at 50 MHz. Dashed lines are used only to associate results for similar systems and do not indicate trends between adjacent points.

4. Nyquist Zone-Based DPD Training

This section presents the implementation of NZ-based DPD training, covering both the training procedure and the receiver-side decoding under NZ constraints. Subsection 4.1 provides a review of NZ-based mapping principles [32]. Subsection 4.2 explains the NZ-based DPD training for an eight-channel multiplex. Subsection 4.3 presents the simulated performance of all DPD training approaches employing an eight-channel composite multiplex.

4.1. Principles of Nyquist Zone Utilization.

Conventional fronthaul SCM receiver architectures require separate frequency conversion hardware for signals located at different IFs, increasing hardware complexity and synchronization requirements [32]. By employing NZ-based mapping, signals can be downconverted to a common IF and processed using a shared receiver architecture, thereby reducing the required frequency-conversion hardware [32].

To clarify this concept, an eight-channel composite signal/multiplex is employed as an example, as depicted in Fig. 8. In Case (A), the eight-channel multiplex is divided into two distinct NZs: the first extends from DC to $f_{s,Rx}/2$, and the second extends from $f_{s,Rx}/2$ to $f_{s,Rx}$, where $f_{s,Rx}$ is the sampling rate employed at the receiver side DDC. In Case (B), the eight-channel composite multiplex is divided into smaller NZs, with two channels allocated per NZ. These NZs extend from DC to $2f_{s,rx}$ in successive intervals of $f_{s,Rx}/2$. For both the two- and four-NZ configurations, channels positioned beyond the first NZ are mapped to mirror locations relative to the first NZ, with the midpoint of the first NZ, i.e., the center frequency of the corresponding channel group, used as the reference frequency. This position ensures correct frequency placement and accurate receiver demodulation. Channel groups require two DDC stages for baseband recovery. For channel groups other than Channel Group 1, the first DDC shifts the group to the first NZ center frequency with a corresponding reduction in the sampling rate, while the second DDC translates each channel individually to DC. For the first NZ channel group, the first DDC performs sampling rate reduction, while the second translates each channel to DC.

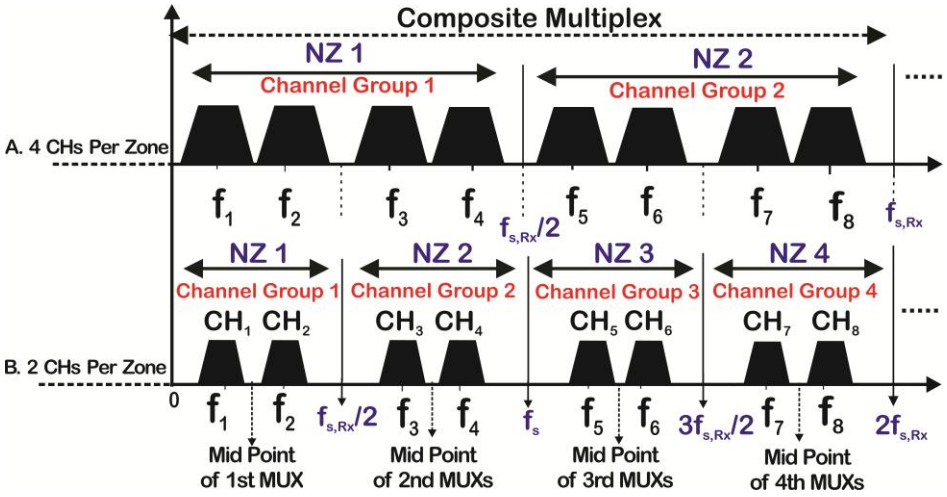


Fig. 8. Conceptual depiction of NZ-based mapping at the transmitter side, for an 8-channel multiplex showing two mapping examples, with two and four NZs, respectively. The $f_{s,Rx}$ is the sampling rate employed at the receiver side DDC.

4.2. Nyquist Zone-Based DPD Training Approach

As with the hybrid approach, the proposed NZ-based DPD remains a waveform-based predistortion technique using time-domain waveform samples for training. However, rather than identifying memory coefficients on a per-channel basis, the proposed approach identifies NZ-specific memory coefficients. Thus, the performance-complexity trade-off arises from the granularity of this NZ-based coefficient identification. In the NZ-based DPD training approach, training is performed independently for each NZ as shown in Fig. 9 (A). A single channel (CH x) is transmitted within each NZ (NZ 1 to NZ n), and the received versions of these channels are used to extract memory polynomial coefficients (with order, Q=5) for the corresponding NZ, while nonlinear effects are ignored (K=0). Using the same received channel, as shown at the top of Fig. 9 (A), the same single channel from NZ 1 is employed to extract nonlinear polynomial coefficients, for the whole composite signal/multiplex, with nonlinear order set to (K=5) while memory effects are disabled (Q=0). For example, for an eight channel multiplex (CH_1 – CH_8), with each NZ containing four channels, CH_1 and CH_5 can be used as the training channels for NZ 1 and NZ 2, respectively. The reuse of memory coefficients within each NZ assumes that the effective frequency-dependent nonlinear amplitude and phase response of the link varies sufficiently slowly across the NZ bandwidth, such that a representative training channel provides an adequate approximation for the other channels in the same NZ. This assumption becomes less accurate in the presence of strong frequency-selective impairments, where additional training channels may be required to adequately represent the memory response.

Fig. 9 (B) shows, the application of the coefficients obtained during training. The memory coefficients extracted for each NZ are applied to the corresponding channel group. Following the eight channel example above, the memory coefficients obtained from CH_1 within NZ 1 are applied to all four channels in the channel group associated with NZ 1, while the memory coefficients derived from CH_5 within NZ 2 are applied to all four channels in the channel group associated with NZ 2. The resulting channel groups are then combined and the nonlinear coefficients obtained from CH_1-NZ 1 during training are applied to the whole composite signal/multiplex to generate the final predistorted output.

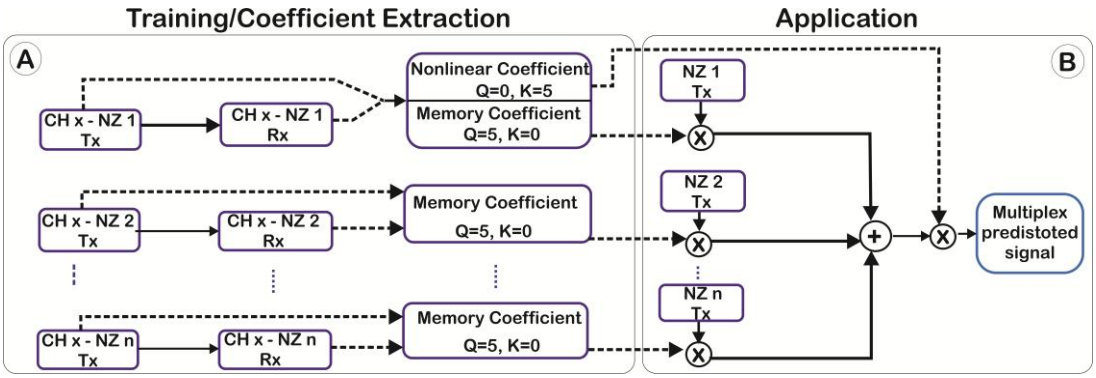


Fig. 9. Conceptual depiction of the NZ-based DPD training approach. Solid lines represent data links; dashed lines represent control information links.

4.3. Simulation-Based Performance Evaluation

Table 1. compares the EVM results from using the NZ-based training approach with those obtained when using the CM-DPD, SC-DPD and hybrid approaches. The multiplex comprises eight channels, with a per-channel bandwidth of 100 MHz. Two cases are evaluated: one with the first channel centered at a low carrier frequency of 50 MHz, and another at a high carrier frequency of 200 MHz. For the higher-carrier frequency case, 200 MHz is used instead of 1200 MHz to accommodate the wider eight-channel multiplex within the usable bandwidth of the modelled optical link.

For both carrier frequency cases, the 2NZs approach provides slightly inferior EVM performance (5.5% at the lower and 5.0% at the higher carrier frequency) to the hybrid approach (4.7% and 3.7% respectively), whereas the 4NZs training achieves nearly identical EVM performance (4.6% and 4.3% respectively). The 4NZs configuration reduces the number of channels sharing each memory-coefficient set, enabling a more localized representation of the frequency-dependent memory response and achieving EVMs of 4.6% and 4.3%, compared with 5.5% and 5.0% for 2NZs at the lower and higher carrier-frequency cases, respectively. This improved linearization comes at the expense of additional NZ-specific training and coefficient updates. Hence, increasing NZ granularity improves the characterization of frequency-dependent memory effects, but with increased implementation complexity. Note that in the eight-channel configuration, the total power is distributed across eight channels instead of four. This reduces the per-channel power relative to the four-channel scenario presented in Subsection 3.1, likely contributing to the observed degradation in EVM performance.

The proposed NZ-DPD has been evaluated through simulation only. However, the simulation framework is benchmarked against the experimental configuration in [32], and the experimentally validated DPD approaches reproduce the general trends observed in simulation. The experimentally achievable channel count and bandwidth are limited by the available test equipment. Consequently, the eight-channel and higher-bandwidth configurations were evaluated through simulation. Hardware implementation and experimental validation of NZ-DPD, including higher channel counts and wider bandwidths, are reserved for future work.

Table 1. Average Error Vector Magnitude (EVM, % RMS) for 16-QAM modulation before and after DPD, for an eight-channel multiplex with a total input power of 19 dBm. Two sets of results are shown, corresponding to center frequencies of 50 MHz and 200 MHz for the first channel in the multiplex.

DPD training approach	No DPD[a]	CM-DPD	SC-DPD	Hybrid	2NZs-DPD	4NZs-DPD
BW /Freq. Carrier (MHz)	100/50					
Avg. EVM (% RMS)	7.3	6.0	5.9	4.7	5.5	4.6
BW /Freq. Carrier (MHz)	100/200					
Avg. EVM (% RMS)	6.6	5.3	5.2	3.7	5.0	4.3

[a]3GPP 16 QAM EVM (12.5 %) Requirements

The reported multi-channel EVM therefore reflects the aggregate impact of in-band distortion and cross-zone intermodulation. This is consistent with previous multi-carrier SCM studies [40], [41], where DPD improved EVM while suppressing adjacent-channel leakage. Individual cross-zone intermodulation products and Adjacent Channel Leakage Ratio (ACLR) are not separately quantified here and are reserved for future investigation

5. DPD Complexity and Power Prediction

The computational complexity quantified through the Multiplication per Input Sample per second (MPIS/s) metric for different DPD training approaches, denoted by Ψ, is given as follows:

$$\Psi = N_M \times R_s \times N_C, \tag{1}$$

where N_M is the number of complex multiply-accumulate (MAC) operations required per sample, R_s is the DPD sampling rate (Hz) and N_C is the total number of DPD coefficients. Note that the coefficient count N_C depends on the deployed DPD training approach. For CM-DPD and SC-DPD, a single DPD coefficient set is employed, giving: $N_C = Q \times K$ for both training approaches. For the hybrid approach, the coefficient count scales with the number of multiplexed channels, N_N, giving: $N_C = (Q \times K) \times N_N$. For the NZ-based approach, the coefficient count scales with the number of NZs, N_Z, giving: $N_C = (Q \times K) \times N_Z$. With the chosen values, each coefficient set contains ($Q \times K = 25$) coefficients. Thus, CM-DPD and SC-DPD require 25 coefficients, while the hybrid and NZ-

based approaches require ($25\times N_N$) and ($25\times N_Z$) coefficients, respectively, using the same parameter values for a fair complexity and performance comparison.

Fig. 10 (right y-axis) shows that MPIS/s increases linearly with sampling rate for all approaches. The hybrid scheme exhibits the highest computational demand, reaching nearly 1.8×10^{12} MPIS/s at 10 GHz, whereas CM-DPD and 4NZ-based approaches require substantially fewer operations.

For a power consumption estimation of the DPD training approach, the employed CMOS technology and its associated energy consumption per operation must be specified. In [23] and [42], power estimations were based on a 28-nm CMOS technology with an energy consumption of approximately 12 pJ per double-precision floating-point operation. Here, we assume a 7 nm CMOS technology with an energy consumption of approximately 4.1 pJ, extrapolated from the scaling trends in [42].

Then, the power consumption for the DPD , denoted by ρ, can be estimated by:

$$\rho = \Psi \times \xi, \tag{2}$$

where ξ is the energy per floating point operation (J).

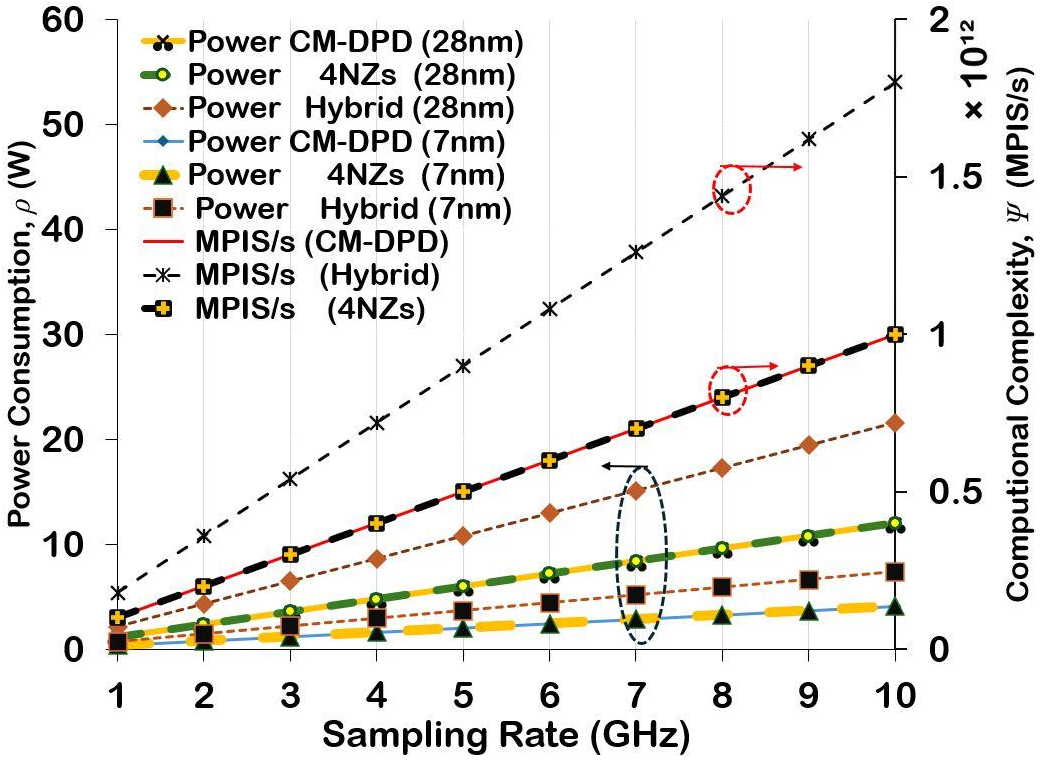


Fig. 10. DPD power consumption (left y-axis) and Multiplications per Input Sample per second (MPIS/s) (right y-axis) versus sampling rate for an eight-channel multiplex. The 28-nm and 7-nm labels refer to CMOS technologies implemented with 28-nm and 7-nm process nodes, respectively.

As expected from (2), power consumption (Fig. 10 (left y-axis)) also increases linearly with sampling rate. The hybrid approach reaches approximately 22 W at 10 GHz in 28-nm CMOS (12 W in 7-nm CMOS), whereas CM-DPD exhibits significantly lower power consumption. The NZ-based approach provides an intermediate solution, achieving power levels close to CM-DPD due to the reduced coefficient count associated with per-zone training.

For comparison, a typical commercial DU server consumes approximately 280 W even when lightly loaded [43]. The proposed hybrid and NZ-based approaches require less than 22 W at a 10 GHz composite sampling rate, corresponding to normalized power efficiency of approximately 2.2 W/GHz. Since this power is consumed only during training rather than continuously, the contribution of these training approaches to the overall DU power budget is modest, particularly for the NZ-based approach.

6. Conclusion

Different training approaches for low-complexity MP-based DPD, targeting the nonlinear behavior of analog transport in a DSP-assisted optical mobile fronthaul with analog transport have been validated through simulation and experimental measurements. This work has investigated per-channel, per-NZ, CM-DPD, and SC-DPD training approaches with different adaptation granularities. The results demonstrate a clear trade-off between implementation complexity and linearization performance. Coarser adaptation granularity reduces implementation complexity at the expense of linearization performance. Experimental validation of the four-channel configuration confirms the simulation trends, with the hybrid per-channel approach providing the best linearization performance. SC-DPD reduces feedback dimensionality and computational burden while providing EVM performance similar to CM-DPD.

The per-NZ approach exploits an existing NZ-based mapping concept as the granularity for DPD adaptation, extending its utility to complexity-aware nonlinear compensation. It provides an effective compromise between performance and complexity, retaining much of the linearization performance of per-channel training while reducing feedback and coefficient-update requirements. Computational complexity and power analysis further show that per-NZ training achieves computational complexity and power consumption comparable to CM-DPD while providing markedly better linearization performance than CM-DPD and SC-DPD. These results demonstrate that NZ-based adaptation provides a scalable approach for high-bandwidth DPD systems requiring both linearity and implementation efficiency.

Future work will include a detailed ACLR evaluation to complement the EVM-based linearization assessment presented in this study. Furthermore, due to limitations of the available experimental test equipment, configurations with eight channels and wider bandwidths were evaluated through simulation only. Experimental validation of the NZ-DPD approach under these extended channel-count and bandwidth conditions will therefore be considered in future work**.**

7. Declaration of generative AI and AI-assisted technologies in the manuscript preparation process.

During the preparation of this work the authors used ChatGPT in order to optimize already written text. After using this tool, the authors reviewed and edited the content as needed and take full responsibility for the content of the published article.

REFERENCES

[1] T. Tao, Y. Wang, D. Li, Y. Wan, P. Baracca, and A. Wang, “6G Hyper Reliable and Low-latency Communication - Requirement Analysis and Proof of Concept,” in *IEEE Vehicular Technology Conference*, Institute of Electrical and Electronics Engineers Inc., 2023. doi: 10.1109/VTC2023-Fall60731.2023.10333792.

[2] A. Larranaga *et al.*, “Fronthaul/Midhaul Networks: Capacity and Latency Requirements Imposed by 6G Disaggregated RANs,” *IEEE Communications Magazine*, vol. 63, no. 5, pp. 86–93, 2025, doi: 10.1109/MCOM.002.2400419.

[3] V. S. Pana, O. P. Babalola, and V. Balyan, “5G radio access networks: A survey,” Jul. 01, 2022, *Elsevier B.V.* doi: 10.1016/j.array.2022.100170.

[4] D. Liu *et al.*, “User Association in 5G Networks: A Survey and an Outlook,” Apr. 01, 2016, *Institute of Electrical and Electronics Engineers Inc.* doi: 10.1109/COMST.2016.2516538.

[5] M. van Hilten and S. Wolfert, “5G in agri-food - A review on current status, opportunities and challenges,” *Comput. Electron. Agric.*, vol. 201, Oct. 2022, doi: 10.1016/j.compag.2022.107291.

[6] S. Rommel *et al.*, “Towards a Scaleable 5G Fronthaul: Analog Radio-over-Fiber and Space Division Multiplexing,” *Journal of Lightwave Technology*, vol. 38, no. 19, pp. 5412–5422, Oct. 2020, doi: 10.1109/JLT.2020.3004416.

[7] L. M. P. Larsen, A. Checko, and H. L. Christiansen, “A survey of the functional splits proposed for 5G mobile crosshaul networks,” *IEEE Communications Surveys and Tutorials*, vol. 21, no. 1, pp. 146–172, Jan. 2019, doi: 10.1109/COMST.2018.2868805.

[8] R. Mackenzie, “NGMN Overview on 5G RAN Functional Decomposition by NGMN Alliance,” 2018. [Online]. Available: https://www.ngmn.org/wp-content/uploads/Publications/2018/180226_NGMN_RANFSX_D1_V20_Final.pdf

[9] R. Puerta *et al.*, “Analog Mobile Fronthaul for 6G and beyond,” *Journal of Lightwave Technology*, vol. 42, no. 21, pp. 7458–7467, 2024, doi: 10.1109/JLT.2024.3435770.

[10] S. Rommel *et al.*, “Real-time high-bandwidth mm-wave 5G NR signal transmission with analog radio-over-fiber fronthaul over multi-core fiber,” *EURASIP J. Wirel. Commun. Netw.*, vol. 2021, no. 1, Dec. 2021, doi: 10.1186/s13638-021-01914-6.

[11] S. Noor *et al.*, “Comparison of digital signal processing approaches for subcarrier multiplexed 5G and beyond analog fronthaul,” *Journal of Optical Communications and Networking*, vol. 12, no. 3, pp. 62–71, Mar. 2020, doi: 10.1364/JOCN.381341.

[12] P. Zhu, Y. Yoshida, A. Kanno, and K. I. Kitayama, “DSP-enhanced radio-over-fiber technologies for 5G-and-beyond wired-wireless convergence,” *Journal of Optical Communications and Networking*, vol. 14, no. 8, pp. 595–605, Aug. 2022, doi: 10.1364/JOCN.455171.

[13] M. U. Hadi, A. Shah, and M. Ijaz, “Experimental Validation of Nonlinearity Mitigation in Analog Radio over Fiber for upcoming 6G Networks Using MSA-Based Digital Predistortion,” in *Proceedings of the IEEE International Multi Topic Conference, INMIC*, Institute of Electrical and Electronics Engineers Inc., 2024. doi: 10.1109/INMIC64792.2024.11004396.

[14] M. Yin, W. Wang, Y. Chen, L. Rong, and F. Li, “Performance Enhanced Cascaded Digital-Analog Radio-Over-Fiber Enabled by Digital Symbol Remapping for 6G Mobile Fronthaul,” *Journal of Lightwave Technology*, vol. 43, no. 8, pp. 3516–3523, 2025, doi: 10.1109/JLT.2024.3511711.

[15] M. U. Hadi, P. A. Traverso, G. Tartarini, O. Venard, G. Baudoin, and J. L. Polleux, “Digital predistortion for linearity improvement of vcsel-ssmf-based radio-over-fiber links,” *IEEE Microwave and Wireless Components Letters*, vol. 29, no. 2, pp. 155–157, Feb. 2019, doi: 10.1109/LMWC.2018.2889004.

[16] P. Assimakopoulos *et al.*, “Flexible and efficient DSP-Assisted subcarrier multiplexing for an analog mobile fronthaul,” *IEEE Photonics Technology Letters*, vol. 33, no. 5, pp. 267–270, Mar. 2021, doi: 10.1109/LPT.2021.3056511.

[17] M. U. Hadi, “Experimental demonstration of transport over fiber using 5G NR with performance enhancement using DPD,” *Opt. Commun.*, vol. 531, Mar. 2023, doi: 10.1016/j.optcom.2022.129226.

[18] W. Tang, M. Hui, T. Liu, D. Shen, and X. Zhang, “A simple envelope-assisted RF/IF digital predistortion model for broadband RoF fronthaul transmission,” *Journal of Lightwave Technology*, vol. 36, no. 19, pp. 4305–4311, Oct. 2018, doi: 10.1109/JLT.2018.2846883.

[19] X. Zhang, T. Liu, and D. Shen, “Investigation of broadband digital predistortion for broadband radio over fiber transmission systems,” *Opt. Commun.*, vol. 381, pp. 346–351, 2016, doi: https://doi.org/10.1016/j.optcom.2016.07.025.

[20] S. A. Bassam, M. H. Helaoui, and F. M. Ghannouchi, “2-D digital predistortion (2-D-DPD) architecture for concurrent dual-band transmitters,” *IEEE Trans. Microw. Theory Tech.*, vol. 59, no. 10 PART 1, pp. 2547–2553, 2011, doi: 10.1109/TMTT.2011.2163802.

[21] R. Zhu, M. Hui, D. Shen, and X. Zhang, “Mach-Zehnder modulator modulated radio-over-fiber transmission system using dual wavelength linearization,” *Opt. Commun.*, vol. 385, pp. 229–237, 2017, doi: https://doi.org/10.1016/j.optcom.2016.09.066.

[22] A. Fayad, T. Cinkler, J. Rak, and M. Jha, “Design of Cost-Efficient Optical Fronthaul for 5G/6G Networks: An Optimization Perspective,” *Sensors*, vol. 22, no. 23, Dec. 2022, doi: 10.3390/s22239394.

[23] J. Wood, *Behavioral modeling and linearization of RF power amplifiers*. Artech House, 2014.

[24] A. Hu, D. G. Byrne, R. Farrell, and J. Dooley, “A Complexity Reduced Non-Uniform Generalized Memory Polynomial Model for Nonlinear Power Amplifier Behavioural Modeling,” in *2019 30th Irish Signals and Systems Conference (ISSC)*, 2019, pp. 1–5. doi: 10.1109/ISSC.2019.8904969.

[25] C. Mateo, P. L. Carro, P. García-Dúcar, J. De Mingo, and Í. Salinas, “Radio-over-fiber linearization with optimized genetic algorithm CPWL model,” *Opt. Express*, vol. 25, no. 4, p. 3694, Feb. 2017, doi: 10.1364/oe.25.003694.

[26] L. A. M. Pereira, L. L. Mendes, C. J. A. Bastos-Filho, and S. Arismar Cerqueira, “Machine Learning-Based Linearization Schemes for Radio Over Fiber Systems,” *IEEE Photonics J.*, vol. 14, no. 6, Dec. 2022, doi: 10.1109/JPHOT.2022.3210454.

[27] L. C. Vieira and N. J. Gomes, “Experimental demonstration of digital predistortion for orthogonal frequency-division multiplexing-radio over fibre links near laser resonance,” *IET Optoelectronics*, vol. 9, no. 6, pp. 310–316, Dec. 2015, doi: 10.1049/iet-opt.2014.0160.

[28] A. Hekkala *et al.*, “Predistortion of radio over fiber links: Algorithms, implementation, and measurements,” *IEEE Transactions on Circuits and Systems I: Regular Papers*, vol. 59, no. 3, pp. 664–672, 2012, doi: 10.1109/TCSI.2011.2167267.

[29] TSGR, “TS 138 211 - V15.2.0 - 5G; NR; Physical channels and modulation (3GPP TS 38.211 version 15.2.0 Release 15),” 2018. [Online]. Available: https://portal.etsi.org/TB/ETSIDeliverableStatus.aspx

[30] M. U. Hadi, K. U. Danyaro, A. AlQushaibi, R. Qureshi, and T. Alam, “Digital Predistortion Based Experimental Evaluation of Optimized Recurrent Neural Network for 5G Analog Radio Over Fiber Links,” *IEEE Access*, vol. 12, pp. 19765–19777, 2024, doi: 10.1109/ACCESS.2024.3360298.

[31] M. U. Hadi *et al.*, “Experimental evaluation of digital predistortion for VCSEL-SSMF-based Radio-over-Fiber link,” in *2018 International Topical Meeting on Microwave Photonics (MWP)*, 2018, pp. 1–4. doi: 10.1109/MWP.2018.8552895.

[32] S. Noor, P. Assimakopoulos, and N. J. Gomes, “A Flexible Subcarrier Multiplexing System with Analog Transport and Digital Processing for 5G (and Beyond) Fronthaul,” *Journal of Lightwave Technology*, vol. 37, no. 14, pp. 3689–3700, Jul. 2019, doi: 10.1109/JLT.2019.2918215.

[33] D. Wake *et al.*, “Design and performance of radio over fibre links for next generation wireless systems using distributed antennas,” in *2010 Future Network & Mobile Summit*, 2010, pp. 1–9.

[34] L. C. Vieira and N. J. Gomes, “Baseband behavioral modeling of OFDM-Radio over fiber link distortion,” in *2012 IEEE International Topical Meeting on Microwave Photonics*, 2012, pp. 188–191. doi: 10.1109/MWP.2012.6474088.

[35] 3GPP, “Directory Listing /ftp/Specs/archive/38_series/38.211/.” Accessed: May 20, 2026. [Online]. Available: https://www.3gpp.org/ftp/Specs/archive/38_series/38.211/

[36] H. Ochiai and H. Imai, “On the distribution of the peak-to-average power ratio in OFDM signals,” *IEEE Transactions on Communications*, vol. 49, no. 2, pp. 282–289, 2001, doi: 10.1109/26.905885.

[37] P. Assimakopoulos, A. Nkansah, N. Gomes, and D. Wake, “Multi-channel signal transmission through radio over fiber architecture,” in *2011 IEEE GLOBECOM Workshops (GC Wkshps)*, 2011, pp. 152–156. doi: 10.1109/GLOCOMW.2011.6162426.

[38] H. Chen *et al.*, “Experimental study on multi-dimensional digital predistortion for multi-band externally-modulated radio-over-fiber systems,” in *2014 IEEE MTT-S International Microwave Symposium (IMS2014)*, 2014, pp. 1–4. doi: 10.1109/MWSYM.2014.6848351.

[39] Q. Wang, B. Song, B. Corcoran, L. Zhuang, and A. J. Lowery, “Real-Time Demonstration of Augmented-Spectral-Efficiency DMT Transmitter Using a Single IFFT,” *Journal of Lightwave Technology*, vol. 35, no. 21, pp. 4796–4803, 2017, doi: 10.1109/JLT.2017.2758401.

[40] B. Yang, H. He, S. Yang, J. Ou, Y. Zhai, and H. Chi, “Analysis on predistortion algorithm for improving adjacent channel leakage ratio of radio over fiber systems,” *Microw. Opt. Technol. Lett.*, vol. 62, no. 4, pp. 1483–1488, Apr. 2020, doi: https://doi.org/10.1002/mop.32216.

[41] Y. Pei *et al.*, “Complexity-reduced digital predistortion for subcarrier multiplexed radio over fiber systems transmitting sparse multi-band RF signals,” *Opt. Express*, vol. 21, no. 3, pp. 3708–3714, 2013, doi: 10.1364/OE.21.003708.

[42] J. Ang and K. Bergman, “ASCAC Subcommittee for the Top Ten Exascale Research Challenges,” 2014. [Online]. Available: https://science.osti.gov/-/media/ascr/ascac/pdf/meetings/20140210/Top10reportFEB14.pdf

[43] Sarat Puthenpura, “Energy measurement and characterization of Open RAN.” Accessed: Jun. 05, 2026. [Online]. Available: https://www.rcrwireless.com/20260323/opinion/readerforum/energy-open-ran